POTENTIAL NOISE SOURCE IDENTIFICATION IN A SINGLE STAGE ROTOR-STATOR COMPRESSOR

Peter HARLEY[1], Raul CORRALEJO[1],
Michael COLLISON[1], Jimmy LIRVAT[1], Oscar WILSBY[2]

[1] *Dyson Technology Ltd., Aero-Acoustic Research Team, Tetbury Hill, Malmesbury SN16 0RP, United Kingdom*

[2] *University of Cambridge, Engineering Dept., Cambridge, United Kingdom*

SUMMARY

State legislation for domestic products has driven the need for noise reduction in low Reynolds number turbomachinery. The current study identifies the prevalent noise source type expected in the current design and potential aerodynamic candidates relating to this. A single stage rotor-stator research axial compressor was explored experimentally and numerically. A quantitative acoustic analysis was performed and a qualitative aerodynamic comparison completed to accompany it. The outcome demonstrated the potential aerodynamic flow features that could be related to the specific energy increase seen in the acoustic spectra.

INTRODUCTION

With recent updates to a range of global state defined domestic appliance legislation, a need has arisen for further reductions to compressor noise levels. Typically, domestic appliance turbomachinery operates in relatively low Reynolds number regimes (<100k), which in terms of compressor design remains a relatively unexplored design space. Ideally turbomachines for home applications are designed to be energy dense to minimise a products footprint, while maintaining an acoustic viability (for example, reducing the tip diameter and increasing the rotational speed can increase power density whilst normally also increasing noise). The purpose of this work was to utilise a range of analysis techniques in order to identify potential noise sources in a single stage rotor-stator research compressor.

A History of Compressor Noise Sources

Typical noise sources in low speed axial fans have been described by many authors. Recently Park et al. [1] explored noise sources in an automotive cooling fan; unsteady RANS CFD was used to determine the pressure based time derivative at key surface locations, and tip leakage interaction

was identified as being potentially responsible for a certain broadband noise feature. Noise generation mechanisms in axial machines have been tackled for decades and were described by Sharland [2]; Sharland concluded that trailing edge vortex shedding was a major source of broadband noise and that "any large-scale turbulence in the flow can increase the noise significantly". Mugridge et al. [3] focused on unsteady turbulent flows on blade rows and the subsequent noise generation. Wright [4] looked at a variety of axial flow machines and compared acoustic trends in an attempt to classify several noise mechanisms. Methods of estimating noise generation from axial machines, moving blade rows, and individual airfoils have been developed by several authors, (Fukano et al. [5], Schlinker el al. [6], and Brooks et al. [7] respectively) but all of them roughly based on the same principle of trailing edge noise estimation. Moreau et al. [8] described how broadband noise mechanisms competed within low speed axial machines. The target of this study was to identify typical broadband noise sources in a low speed axial machine and explore how those aerodynamic noise sources vary off-design. The finer details of noise generation mechanisms were not considered in this work; it was assumed that Sharland's analogy of large-scale turbulence being a potential source of noise was true and therefore the existence of well-known compressor aerodynamic flow features were assessed using numerical and experimental methods.

Wright [4] compiled a range of axial flow machines in order to group noise mechanisms; they determined that various rotor devices could be described by a common characteristic spectrum, and that aerodynamic details can be interpreted from the acoustic spectra; it is worth noting that Wright's datasets were all in free field propagation scenarios whereas the current work focuses on turbomachines contained within a rigid duct (propagation described by Nelson et al. [9]. Wright plotted the sound pressure level for a range of measurements from different designs, sources and applications and found a remarkable collapse as shown in Figure 1; although crude Wright suggested that at low tip speeds noise scaled with U^3, mid speeds aligned better with U^5, and at high tip speeds scaled with U^8. Wright argued that the myth of all rotor noise increasing with U^6 was dispelled by this plot.

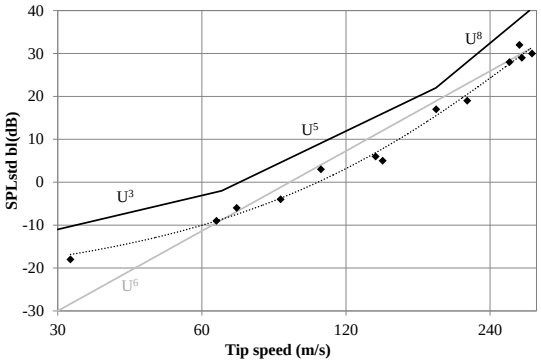

Figure 1: Peak broadband noise for a range of axial machines versus tip speed, Wright [4]

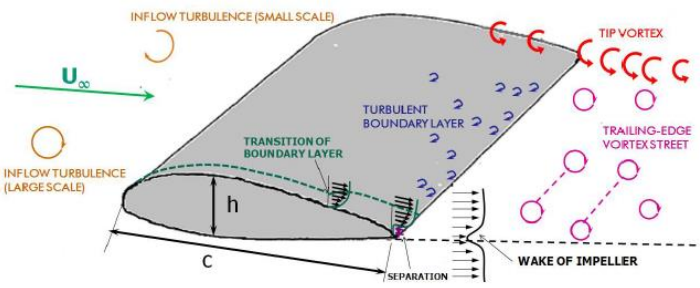

Figure 2: Noise sources in a typical blade

Wright also suggested a minimised broadband noise concept which stated that for a given loading, the tip speed should be minimised, solidity should be maximised, and a maximum incidence angle of 4 degrees permitted; in essence aerodynamically this means that the tip diameter should be maximised to minimise the required turning for a given loading according to the Euler turbomachinery work equation, that blade loading should be minimised through increased solidity, and that stall due to excessive positive incidence should be avoided.

In a low speed ducted axial machine dipole sources dominate; typical aerodynamic noise sources found in such a machine are shown in Figure 2. In a low Reynolds number device, further effects are found such as transition and separation. Classic separations are found at the leading edge, on the suction surface, and toward the hub-suction side corner. In a low speed axial machine the tip vortex

can fill a significant portion of the flow passage causing notable levels of shear and can impact on the next blade causing a further noise source (also referred to as double leakage).

It is important to recognise that sound power level is only one descriptor of the noise. The design point broadband energy distribution and tonal content are as important as off-design operating point noise when a machine is required to have a wide operating envelope. The quality of the noise must also be considered during product design and for this the semantics of sound quality need to be described; although not assessed in this study it has been recently demonstrated by Feldmann et al. [10].

During in-house development of low speed axial and mixed flow machines the typical off-design sound power level curve has been found through experience to be similar to that shown in Figure 3. Normally a minimum noise bucket exists with an adjacent relatively flat section around peak efficiency. Toward stall the sound power level increases rapidly whereas toward choke it increases slowly. This work aimed to explore why noise increases toward stall and choke, why there is a flat section around peak efficiency, and why the minimum noise bucket does not align with peak efficiency in the current research stage.

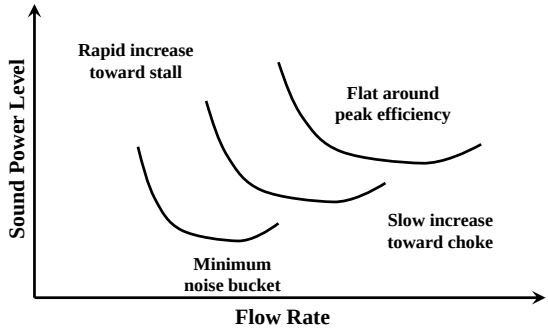

Figure 3: Typical sound power level curve

METHODOLOGY

The compressor used in this study contained a single rotor-stator blade row. The impeller was designed at the hub and shroud from circular arc constant thickness profiles; the compressor geometry is presented in Table 1. The tip gap was 0.5 mm and a cross section of the compressor is provided in Figure 4.

Table 1: Compressor geometry

	Rotor hub	Rotor shroud	Stator hub	Stator shroud
LE [deg]	-67	-69	52	49
TE [deg]	-38	-54	23	0
LE t [mm]	1.0	1.0	1.0	1.5
TE t [mm]	1.0	1.0	2.1	1.5
Radius [mm]	29.3	50.0	29.3	50.0
Chord [mm]	28.8	36.6	37.0	33.0

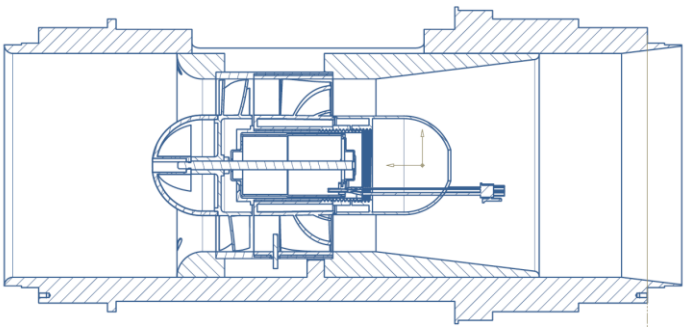

Figure 4: Compressor cross section

The compressors were driven by Shinano-Kenshi mass produced electric motors. PID control was used to manage the speed of the motor and power draw was calculated through measurement of the current draw. Each of the motors used were measured on a dynamometer in order to judge the

electrical power draw versus the shaft power so that the isentropic efficiency of the stage could be calculated.

A series of different information sources where utilised to build the required database of information for this investigation. The experimental method used an in-house ducted research compressor setup as shown in Figure 5. The measurement method was based on ISO 5136 [11] and has the capacity to measure flow rate through the inlet orifice plate, pressure rise across the compressor, system efficiency, as well as sound power level based on upstream and downstream microphones; this study focused only on the pressure rise (Furness Model FCO318), upsteam and downstream noise measurements (Bruel & Kjaer 4189), and the mass flow rate (orifice plate based on ISO 5167 [12]).

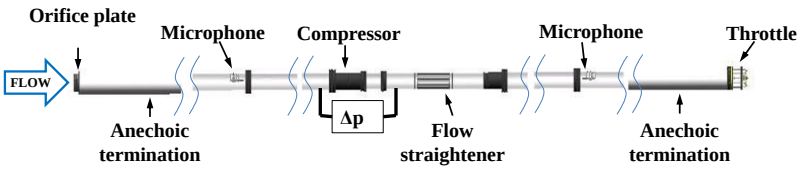

Figure 5: Experimental setup according to ISO 5136

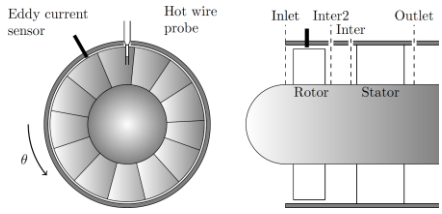

Figure 6: Hotwire installation

Further detailed measurements were taken using an in-house hotwire traverse system that permits radial, axial, circumferential and rotational positioning. The hotwire measurements were completed using a Dantec Streamline Pro CTA system along with general purpose Dantec 55P11 miniature hotwire probes, and phase-lock triggering was achieved using a micro-epsilon DS1(04) eddy current sensor coupled with a DZ140 controller; the hotwire and eddy current sensor insertion method is shown in Figure 6 (Inter and Inter 2 were 27.6 mm and 21.1 mm respectively downstream from the leading edge, Inlet was 8.9 mm upstream of the leading edge). In order to determine the flow angle the hotwire was rotated until a maximum velocity was found prior to any signal acquisition; this was repeated for every spanwise measurement location and axial position. Phase-locked rotor wakes were constructed using the eddy current sensor clock signal from the passing blade to re-index the hot wire voltage from time to passage phase. The resolution of the phase locked averages was governed by the radial increments and the sampling frequency of the anemometer system. At 4400 rpm and 100 kHz the circumferential resolution was 105 points per passage. The radial resolution was in excess of 40 points per passage corresponding to 0.5 mm steps at midspan and 0.1 mm steps in the hub and shroud boundary layers; averages where collected over 20 seconds corresponding to approximately 1467 impeller rotations or 19067 passages at 4400 rpm.

In full, time averaged flow rate, pressure rise, efficiency, and sound power level was collected, and unsteady information was captured with the hotwire at multiple locations (as shown in Figure 6) as well as the upstream and downstream microphones. To assess repeatability a series of four compressor builds was completed and each of the compressors tested on the same test rig with a variety of operators and daily conditions; the data presented represents the complete sample.

Further insight was gained through the use of CFD. A multitude of variants were generated again to assess their ability to accurately represent the flow physics that could explain the off-design sound power level trends. ANSYS CFX was used to assess a series of turbulence models, namely k-ε, SST, and SST-Rθ. The full experimental duct was included in the RANS simulations including a flow straightener as shown in Figure 5; the mesh cell distributions are provided in Table 2. The mesh was unstructured and was generated used ANSYS Mesh; it was split up into a stationary inlet domain, frozen rotor rotating impeller domain, and a stationary outlet domain (also containing the stator blades). A frozen rotor interface was used between the inlet and impeller domains, and a mixing plane (stage interface) was used between the impeller and outlet domains. The mixing plane was deemed acceptable as the distance between the impeller and stator blades in this design was relatively large (approximately the same axial length as the impeller); legacy experience of hot wire

measurements suggested that the impeller wake would be relatively weak upon reaching the stator blades. As this was a steady simulation, no rotor-stator interaction would be physically modelled and therefore the mixing plane model was deemed acceptable. On the inlet domain y+ was not controlled and the automatic CFX wall function was applied. Within the impeller domain y+ was maintained below 2 throughout, and based on experience 14 cells were included in the tip gap. In the outlet domain y+ was varied; around the stator blades y+ was controlled below 4, and this expanded beyond the outlet of the stage until the CFX automatic wall function was applied. A mesh dependency study was carried out using the SST turbulence model to ensure macro performance parameters such as pressure rise were no longer varying, and the mesh was defined based on minimising the simulation time required.

Table 2: CFD mesh properties

	Inlet Domain	Rotating Domain	Outlet Domain
ANSYS CFX – RANS (tetrahedral)	1.4M	12.7M	12.1M

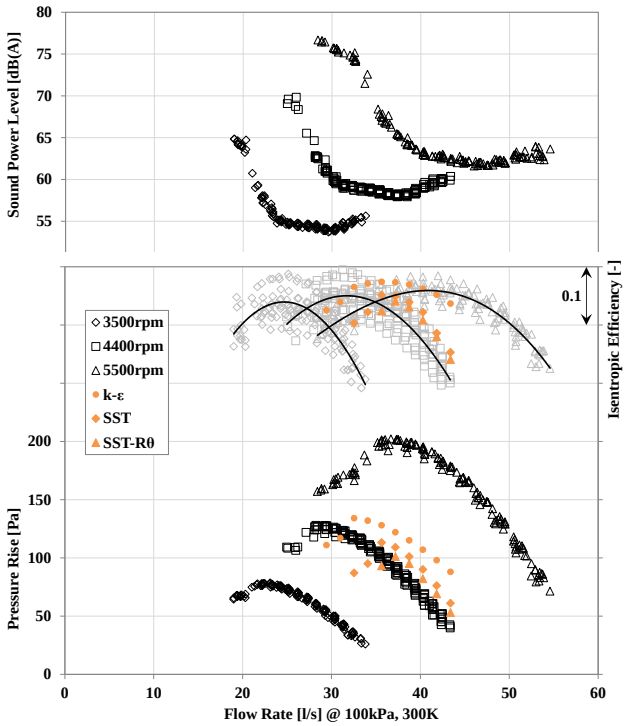

Figure 7: Compressor performance map

RESULTS & DISCUSSION

Aerodynamic Assessment

The performance map from the current compressor is presented in Figure 7; this represents multiple builds of the same geometry as well as multiple repeat experiments on different days by different operators of the various builds. Three rotational speeds were tested, 3500 / 4400 / 5500 rpm. The pressure rise and sound power level measurements had good repeatability across all measurements, although the efficiency measurement had large variability. The isentropic efficiency was reverse calculated based on dynamometer measurements of all of the individual motors along with power draw measurements through a desk power supply. The efficiency measurements followed a normal distribution and therefore best fit curves have been used to best represent the populations for each rotational speed.

Three variants of RANS simulations were completed of the fully ducted compressor at 4400 rpm; the three variants used the k-ε, SST, and SST-Rθ turbulence models, the results from these are shown in Figure 7. The CFD models all stalled at a higher flow rate than seen experimentally. The k-ε model remained stable at the lowest flow rates, whereas the SST models stalled at high flow rates (even before peak efficiency). k-ε over-predicted the pressure rise and efficiency highlighting that the total pressure losses were not accurately captured and potentially vital flow features were missed, furthermore the work input was over-estimated by the k-ε model. The SST turbulence model still over-predicted the work input but the total pressure losses simulated within the rotor reduced the pressure rise and efficiency to more realistic levels. Finally the SST-Rθ model has similar work input to the others but further increased the pressure losses in the flow passage.

The hotwire measurements are provided in Annex A – Figure 11 where they are compared against all available CFD simulations. The inlet flow was captured well with all simulations as would be expected. The post-impeller pre mixing plane location demonstrated the capacity of each of the turbulence models to capture the impeller flow field. At the highest measured/simulated flow rate of 42 l/s the post impeller velocity and flow angles aligned well for the majority of the span, however it can be seen that between 5-20 % of the span what appeared to be a 'hub-corner' separation was causing deviation; the measured shape of the flow feature aligned well with that described by Hah et al. [14] providing some confidence in the hub-corner separation hypothesis. None of the RANS simulations captured an impeller hub-corner separation at 42 l/s, but the flow field in the remainder of the span was captured with some accuracy. Although hotwire measurements were not collected post stator the CFD data is presented in Annex A – Figure 11 to give an indication to the stator flow physics. At 42 l/s there was significant disparity across the different turbulence models whereby the SST models predicted a stator leading edge pressure side separation and the k-ε model predicted a stator hub-corner separation. The post stator results should only be used as speculative as they were not validated in this study.

At 38 l/s the measured hub-corner separation had grown to engulf up to 30 % of the span. k-ε provided the most accurate overall spanwise velocity distribution at 38 l/s, whereas deviation from the measured values became visible toward the shroud for the SST turbulence models. In the stator the SST models suggested that the leading edge pressure side separation still existed but was reduced in magnitude, whereas the k-ε model suggested that the hub-corner separation increased in magnitude.

At 32 l/s the SST turbulence models had become unstable, this was particularly evident when comparing the CFD generated flow field against the phase-locked averaged experimental data as shown in Annex B Figure 13. The SST turbulence models suggested the presence of stall cells whereas the k-ε model remained stable; this appeared to be due to the over-estimation of the tip leakage vortex as seen in the hub-shroud plots for 32 l/s above a span of 60 % (Figure 11). Based on the current triggering method for phase-locking it was impossible to determine if stall cells did exist, and if stall cells did exist they would be smeared circumferentially using the current technique; a potential example of this was seen at 29 l/s in the phase-locked averaged post impeller measurements by the high velocities close to the shroud. Additional blockage was seen toward the hub (Annex B – 32 l/s at Inter2 location) as was evident by the higher flow angle; this resulted in a lower axial velocity toward the hub which in the experimental cases appeared to accelerate the flow toward the shroud and this potentially stabilised the flow near the shroud at lower flow rates. The CFD simulations did not predict the blockage toward the hub and were therefore more susceptible to low momentum flow stall toward the shroud. Post stator, only the SST-Rθ turbulence model was now predicting any separation and the k-ε and SST were now roughly in agreement; these models predicted continued growth of the hub-corner separation.

Further clarity can be gained from Annex A – Figure 12 detailing impeller and stator incidence and deviation angles. The hub-corner separation in the impeller caused large deviation toward the hub (up to approximately 10 deg), whereas the mid-span deviation varied between approximately

6-8 deg; this was in line with what would be expected according to Carter's rule as defined by Cetin et al. [15] and also aligned with previous experience of low Reynolds numbers MISES simulations (Corralejo et al. [16]). Due to the hub-corner separation the stator incidence at the design flow rate of 32 l/s was positive toward the hub but negative above 40 % span; this was due to the flow above 40 % span being accelerated by the blockage toward the hub. Toward 38 l/s and 42 l/s the majority of the flow above 30 % span had a significantly negative incidence angle, up to approximately -18 deg at 42 l/s. Such negative incidence angles caused significant separations on the leading edge and are discussed in the later section relative to their acoustic properties.

Acoustic Assessment

The aim of this study was to identify aerodynamic features that potentially pertained to variations in the noise produced across the compressor map. In the previous section the aero-thermal performance of the machine was discussed as well as the capacity of various steady state RANS simulations to capture the flow physics accurately; for the acoustic assessment to follow only the k-ε and SST turbulence modelling was considered. The average SWL for all operating points is presented in Figure 8; it can be seen in Figure 7 that the minimum noise did not align with the peak efficiency, and that the noise increase rate toward choke was much less than that toward stall. The remainder of this document will aim to explore potential aerodynamic features that describe exactly these effects.

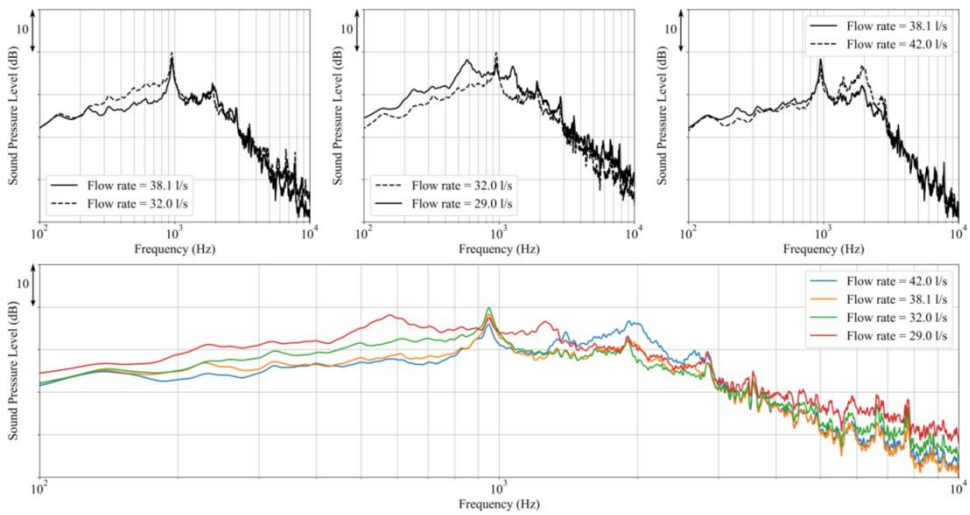

Figure 8: A-weighted SPL spectra at 4400 rpm across several flow rates

Peak Efficiency not Aligning with Minimum Noise – The average (A-weighted) spectral sound pressure level of both upstream and downstream microphones is shown in Figure 8 for a range of flow rates at 4400 rpm. The minimum noise was measured at approximately 38 l/s which did not align with peak efficiency. Comparing the spectrum at 32 l/s (approximately peak efficiency) with that at 38 l/s (Figure 8 top left) there was a clear increase in energy between 200-900 Hz. Aerodynamically the impeller hub-corner stall increased in size from 30 % to 50 % of the span (Annex A – Figure 12) between the flow rates and this was suspected as a major contributor to the measured noise increase. Furthermore the tip leakage magnitude increased between 38 l/s and 32 l/s as can be seen in the phase-locked average contour plots (Annex B Hotwire); increased levels of tip leakage flow was expected to increase the sound power level. The incidence on to the impeller varied from approximately 0 deg (averaged over the span) at 38 l/s to approximately +4 deg at 32 l/s (Annex A – Figure 13). The positive incidence at 32 l/s resulted in a notably thicker suction side boundary layer in the k-ε RANS simulations (Figure 9a) suggesting that trailing edge noise would also have been expected to increase. The k-ε simulations predicted a hub-corner separation in the stator at both 32 l/s and 38 l/s, and this grew in size from approximately 20 % span at 38 l/s to 40 % span at 32 l/s (Annex A – Figure 11); this was also expected to be a contributor to the noise

increase. Finally the k-ε simulation predicted a suction side separation at 32 l/s and not at 38 l/s as shown in Figure 9b, and this was expected in to increase trailing edge noise from the stator blades. In full five potential aerodynamic noise sources were identified that could be contributing to the frequency range notes above, these were:

- Impeller hub-corner separation increased
- Impeller tip leakage flow increased
- Impeller suction side boundary layer thickened
- Stator hub-corner separation increased
- Stator suction side separation

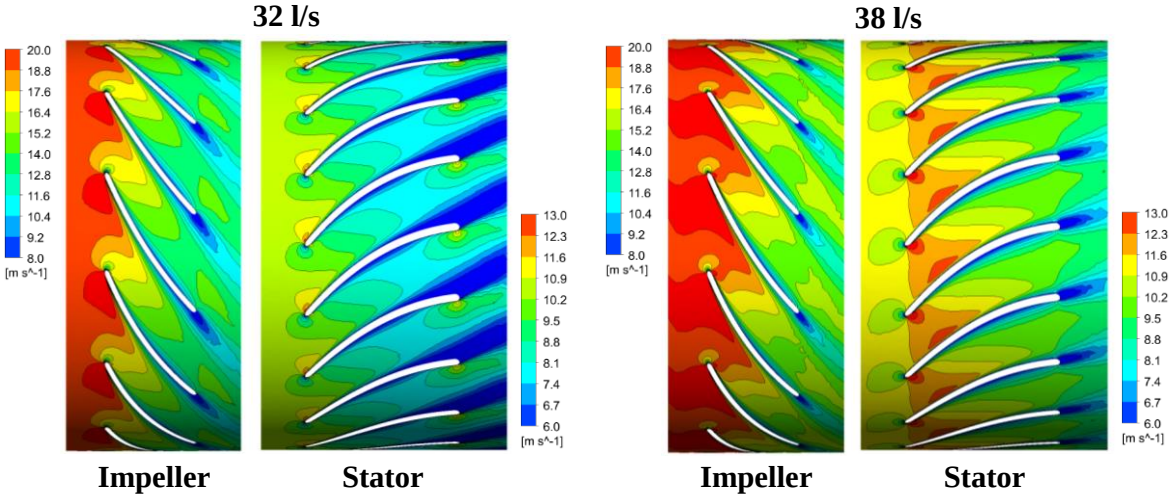

Figure 9: Velocity at 50 % span (k-ε), 32 l/s left and 38 l/s right, (a) impeller, (b) stator

Rapid Noise Increase toward Stall – It was difficult to determine if the early onset of stall cells was prevalent at 32 l/s, although the k-ε simulations certainly suggested a potential instability; as described earlier the hub-corner separation within the impeller could have stabilised the shroud and delayed the onset of stall. Referring again to the spectra shown in Figure 8 (top middle), the change between 32 l/s and 29 l/s is considerably more broadband. A series of humps and their harmonics emerged as the dominant noise sources suggesting discrete pressure fluctuations circumferentially existed; an obvious example of a harmonic emerged between 450 Hz and 750 Hz. The instability predicted by the k-ε simulation at 29 l/s is shown in Annex B; this shows the numerical existence of one stalled lobe toward the shroud. Based on the centre frequency of 600 Hz, it suggested that a stalled region was rotating at approximately 60 % of the impeller rotational speed. The experimental phase-locked averaging technique did not permit the capturing of stall lobes, additional high frequency pressure measurements would have been required around the impeller shroud in order to phase-lock any rotating instability modes relative to any discrete blade passage. The onset of the stalled region was hypothesised to be due to the tip leakage vortex landing close to the leading edge of the adjacent blade passage, causing poor incidence angles on the adjacent blade and eventual stall on that blade, and in-turn setting up the classic circumferentially propagating rotating stall scenario. There was an additional energy increase above 5 kHz between 32 l/s and 29 l/s, however after A-weighting this energy did not contribute largely to the overall SWL and was therefore not investigated in this work. Therefore the potential aerodynamic feature that led to the rapid increase in SWL toward stall was thought to be impeller stall which resulted in the unsteady non-axisymmetric loading of the impeller blade row and in-turn scattering from the impeller trailing edge and stator blades.

Noise Increase toward Choke – Referring again to the difference between the measured spectra (Figure 8 top right) between 38 l/s (minimum noise) and 42 l/s (toward choke) there was a clear increase in energy between 1500 Hz and 2500 Hz. Wright's [4] work suggests that the flow features

that cause similar energy spectra are laminar shedding. The hotwire data collected only investigated the impeller, and based on this the cleanest impeller flow field was measured at 42 l/s, therefore it can be hypothesised that the noise increase did not originate from a macro aerodynamic feature in the impeller. It was therefore thought that the noise toward choke could be originating in the stator blade row. Based on the hotwire measurements the stator incidence angles were calculated and at 42 l/s were up to -18 deg above 30 % span; this aligned well with the SST simulations. The k-ε model had an incidence angle of up to -15 degs and did not predict a pressure side separation, but instead suggested a strong thickening of the pressure side boundary layer. The SST models on the other hand with higher incidence angles predicted an unsteady separation at the leading edge of the stator blades as seen in Figure 10. The feature also existed at 38l/s in both the SPL spectrum (Figure 8) as well as in the CFD, although at 38 l/s it was smaller; therefore it was postulated that the increased energy between 1500 Hz and 2500 Hz was due to the separation at the leading edge of the stator and the subsequent unsteady loading on the blade.

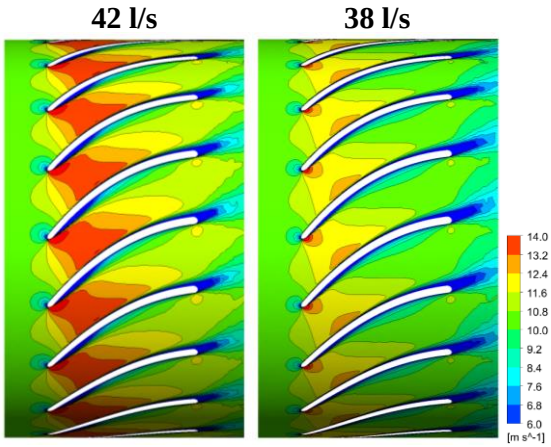

Figure 10: Stator velocity at 50 % span (SST), 42 l/s left and 38 l/s right

CONCLUSIONS

An assessment of a low Reynolds number single stage rotor-stator axial compressor was conducted. Several builds of the same geometry were tested under similar conditions to ensure repeatability of the test method. The pressure rise, sound power level, and sound pressure level spectra were measured with good repeatability although the efficiency repeatability was weak with a fairly normal distribution. An aerodynamic assessment was used to gauge the validity of the CFD simulations and it was demonstrated that an impeller hub-corner separation existed in reality but was not captured by the RANS simulations. Furthermore it was shown that the SST turbulence models stalled at high flow rates, this was hypothesised to be due to the overestimation of the tip leakage flow. An acoustic assessment was carried out to demonstrate the off-design aerodynamic flow features that were expected to be contributing to the overall sound power level; key acoustic contributors were identified as hub-corner separations, tip leakage flows, boundary layer thickness, and any large-scale turbulence generated from separation. In future it is not expected that RANS CFD alone is sufficient to answer these questions as it was in places missing key fundamental flow physics which limited the ability to truly identify all noise sources. With knowledge of the limitations SST worked well while the compressor was operating close to choke, however when operating close to stall k-ε worked best as the SST model grossly over-predicted the tip leakage flow.

BIBLIOGRAPHY

[1] M. Park, D. Lee – *Sources of broadband noise of an automotive cooling fan*, Applied Acoustics, Vol. 118, **2017**

[2] I. J. Sharland – *Sources of noise in axial flow fans*, Journal of Sound and Vibration, Vol. 1, Issue 3, **1964**

[3] B. D. Mugridge, C. L. Morfey – *Sources of noise in axial flow fans*, Journal of the Acoustical Society of America, Vol. 55, **1972**

[4] S. E. Wright – *The acoustic spectrum of axial flow machines*, Journal of Sound and Vibration, Vol. 45, Issue 2, **1976**

[5] T. Fukano, Y. Kodama, Y. Senoo – *Noise generated by low pressure axial flow fans, I: Modeling of the turbulent noise*, Journal of Sound and Vibration, Vol. 50, Issue 1, **1977**

[6] R. H. Schinkler, R. K. Amiet – *Helicopter rotor trailing edge noise*, NASA CR-3470, **1981**

[7] T. F. Brooks, D. S. Pope, M. A. Marcolini – *Airfoil self-noise and prediction*, NASA RP-1218, **1989**

[8] S. Moreau, M. Roger – *Competing broadband noise mechanisms in low-speed axial fans*, AIAA Journal, Vol. 45, Issue 1, **2007**

[9] P. A. Nelson – *Aerodynamic sound production in low speed ducts*, Journal of Sound and Vibration, Vol. 79, Issue 2, **1981**

[10] C. Feldmann, T. Carolus, M. Schneider – *A semantic differential for evaluating the sound quality of fan systems*, ASME Turbo Expo 2017, GT2017-63172, **2017**

[11] ISO 5136 – *Acoustics - Determination of sound power radiated into a duct by fans and other air-moving devices - In-duct method*, **2003**

[12] ISO 5167-2 – *Measurement of fluid flow by means of pressure differential devices inserted in circular cross-section conduits running full -- Part 2: Orifice plates*, **2003**

[13] F. Mendonca – *Large-Eddy Simulation for Acoustics*, Cambridge University Press, **2007**

[14] C. Hah, J. Loellbach – *Development of hub corner stall and Its Influence on the performance of axial compressor blade rows*, Vol. 121, Issue 1, **1999**

[15] M. Cetin, A. S. Ucer, C. Hirsch, G. K. Serovy – *Application of modified loss and deviation correlations to transonic axial compressors*, AGARD Report No. 745, **1987**

[16] R. Corralejo, P. X. L. Harley – *Smith diagram for low Reynolds number axial fan rotors*, 12th European Turbomachinery Conference, Stockholm, Sweden, **2017**

ANNEX – A

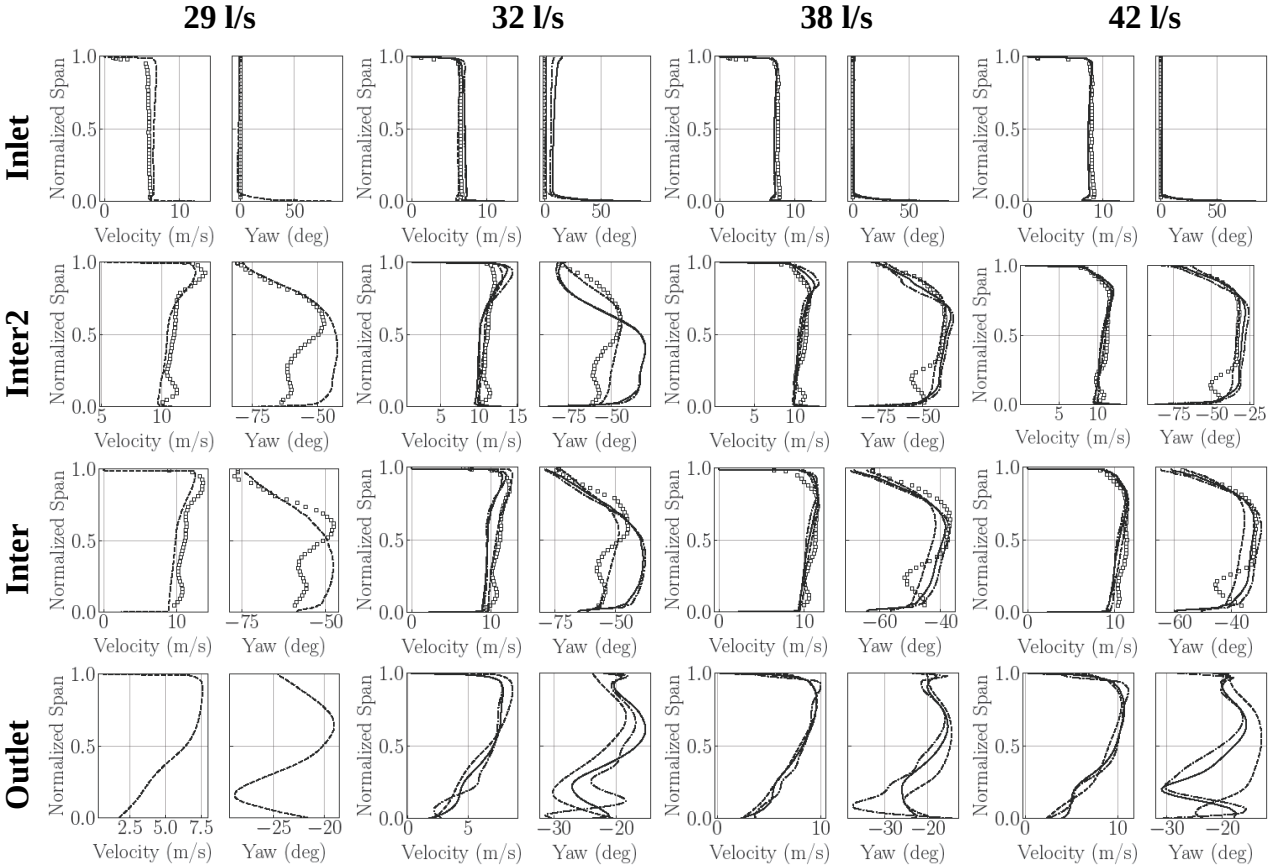

Figure 11: Traverse data comparison (points – hotwire, solid line – SST, dashed line – k-ε, dash-dot line – SST-Rθ)

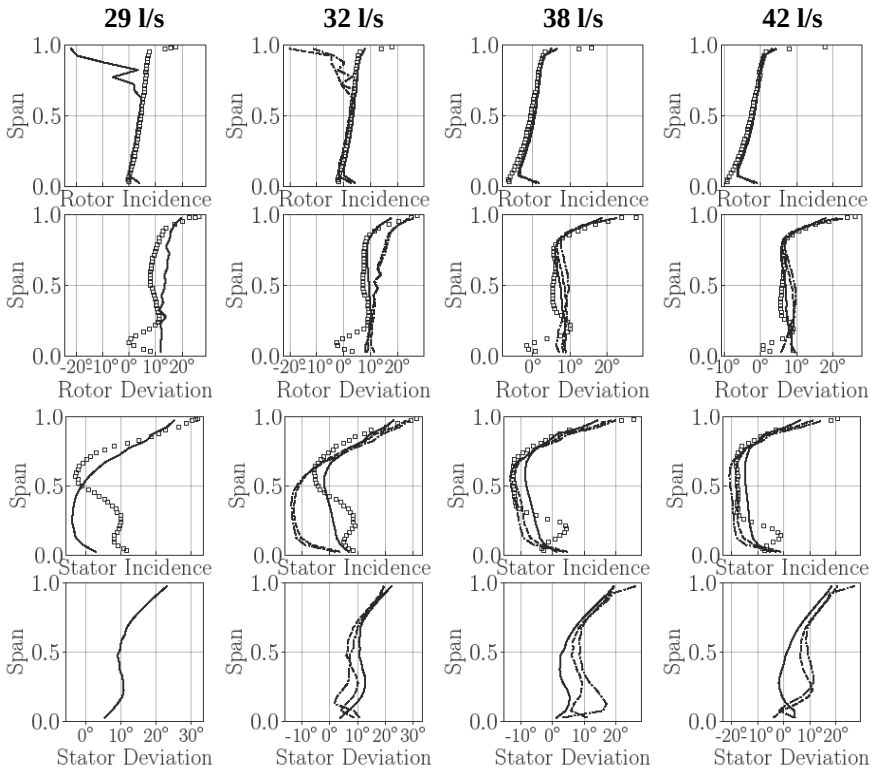

Figure 12: Calculated incidence and deviation angles on the impeller and stator

ANNEX – B

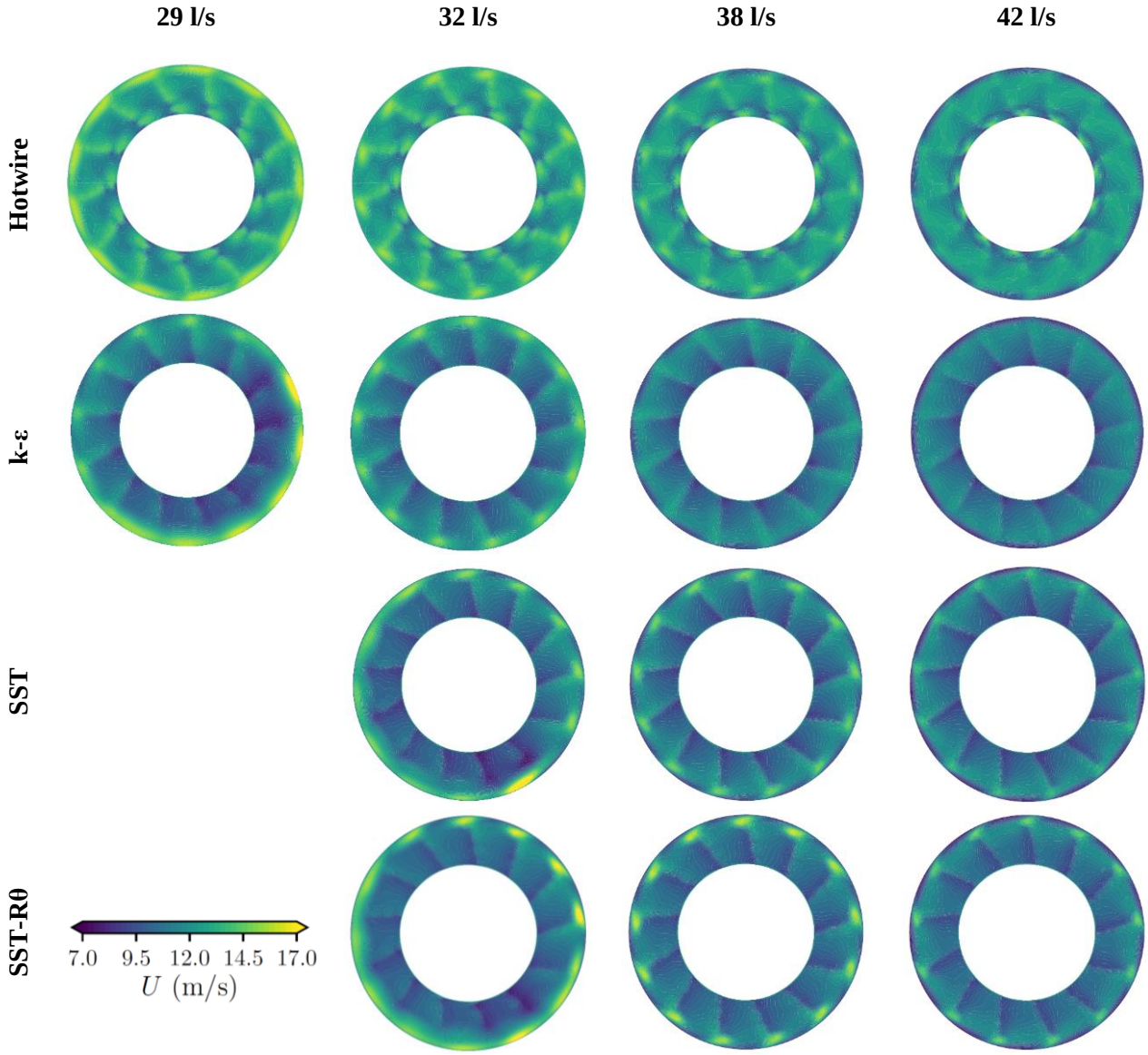

Figure 13: Inter rotor-stator plane velocity comparison